

We are IntechOpen, the world's leading publisher of Open Access books Built by scientists, for scientists

6,900

Open access books available

186,000

International authors and editors

200M

Downloads

Our authors are among the

154

Countries delivered to

TOP 1%

most cited scientists

12.2%

Contributors from top 500 universities



WEB OF SCIENCE™

Selection of our books indexed in the Book Citation Index
in Web of Science™ Core Collection (BKCI)

Interested in publishing with us?
Contact book.department@intechopen.com

Numbers displayed above are based on latest data collected.
For more information visit www.intechopen.com



Hyperelastic Modeling of Rubber-Like Photopolymers for Additive Manufacturing Processes

Giovanni Berselli¹, Rocco Vertechy², Marcello Pellicciari¹
and Gabriele Vassura³

¹*University of Modena and Reggio Emilia*

²*PERCRO Laboratory, Scuola Superiore Sant'Anna*

³*University of Bologna
Italy*

1. Introduction

This chapter addresses design issues of components realized with rubber-like PhotoPolymers (PP) recently introduced in Rapid Prototyping. In particular, the determination of accurate, hyperelastic, constitutive models which describe the PP behavior is discussed in detail. In fact, Stereolithography and Polyjet processes allow the production of highly flexible objects by using photosensitive resins whose mechanical properties are, in some cases, similar to natural rubber. These parts, being fabricated with an additive approach, eventually represent a final product instead of a mere 'prototype'. Therefore, the term Additive Manufacturing (AM) might be used in substitution to Rapid Prototyping (Gibson et al., 2010) in order to underline a closer link to the end-use component. From a designer's point of view, AM technologies offer the possibility, before unknown, to customize and singularly optimize each product for the end user, such that focused design methods are needed.

In the case of rubber-like PP, the considered materials usually experience deviatoric (isochoric), fully reversible deformations which can be well described by hyperelastic constitutive theories capable of dealing with large (finite) strains (Holzapfel, 2001). The capability to undergo finite deformations may intrinsically solve several functional design requirements but this requires an accurate representation of the material behavior through proper constitutive models. Unfortunately, the only data which are available (e.g. data from Objet Geometries Ltd., <http://www.objet.com/docs/>) are limited to basic material properties, namely tensile strength, tensile modulus at few reference stretch ratios, compression set, and hardness. Hence, the correct design and verification of AM rubber-like products become impossible or, at least, very difficult. For example, every shape optimization through nonlinear Finite Element Analysis (FEA) requires a constitutive material law (i.e. a relation between stress and deformation) as a key input of the numerical model. In the same way, the calculation of hardness and friction influence on the product contact behavior requires a detailed description of its deformation state for given applied loads (Shallamach, 1952). If a rough estimate of any stress-strain field based on the aforementioned data may be acceptable for the first-attempt sizing of a prototype, nonetheless the design for direct manufacturing of

end-products through AM technologies becomes critical. In this contest, the development of virtual prototypes capable of correctly predicting the system response in the case of non-linear large deformations is fully motivated and may lead to successful innovations. Therefore, the knowledge of the numerical and experimental routines used to determine the material hyperelastic parameters becomes fundamental and represents the foundation for any AM custom design methods.

In summary, the chapter outline is the following:

- Section I summarizes relevant equations and definitions of continuum mechanics. Typical hyperelastic models, which can be used to describe AM materials, are reviewed along with their intrinsic limitations.
- Section II discusses the experimental tests which are necessary to determine the material constitutive parameters. A Matlab code, implemented by the authors, which may be used to numerically fit the experimental data is reported. As said, the correct determination of the material constitutive parameters represents the first step in any design optimization routine achieved by means of FEA.
- Section III presents a design case study: rubber pads made of photosensitive polymers are studied through non-linear FEA (Berselli & Vassura, 2009.; Piccinini et al., 2009.). The case study highlights that the use of different constitutive laws leads to different numerical solutions for a given boundary-value problem.

2. General remarks on hyperelastic models for rubber-like polymers.

A constitutive equation is a physically-based mathematical model relating stress and deformation. Among the many possible theories provided in the literature (refer to Holzapfel (2001) for a review), the choice of the relation which best describes the actual material behavior is based on both empirical observations and the capability to easily handle the formulation. With reference to the class of materials considered here, at a macroscopical level, it is observed that:

- The PP can experience large fully reversible deformations.
- At low deformation rates, hysteresis and viscous effects are negligible.
- The volume of the specimen does not change under arbitrarily high loads.
- There exist preferred directions of damage since the manufacturing process of the final product is based on the subsequent deposition of thin layers (16 μm).

Therefore, it is reasonable to assume a *hyperelastic, incompressible* behavior in quasi-static conditions. In addition, depending on manufacturing quality, layers direction and applied loads, the material might be considered either *orthotropic* or *isotropic*. In the following, a homogenous *isotropic* behavior is assumed. The material characterization on the basis of orthotropic constitutive models is currently under development.

2.1 Basic equations

Concerning hyperelastic isotropic materials, it is postulated the existence of a Helmholtz free-energy function, W , which is defined per unit volume in the undeformed configuration of the material. The scalar value, W , is called *strain-energy function* if it depends exclusively on the material deformation. For instance, one can express the strain energy as $W = f(\mathbf{B})$ or $W = f(\mathbf{F})$, where $\mathbf{B} = \mathbf{F}\mathbf{F}^T$ is the left Cauchy-Green (or Finger) deformation tensor and \mathbf{F} is the the deformation gradient tensor. Referring to Fig. 1, the tensor \mathbf{F} maps an infinitesimal line element in the undeformed configuration, dx' , to a corresponding line element, dx , in the

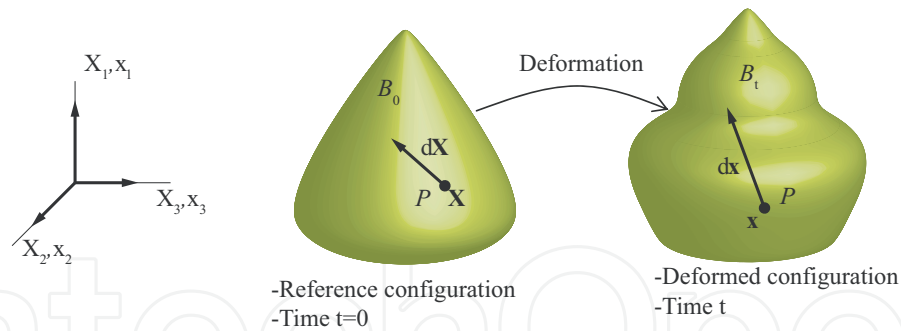


Fig. 1. Deformation schematic. Adapted from Holzapfel (2001).

deformed configuration, that is (index notation):

$$dx_i = \frac{\partial x_i}{\partial X_j} dX_j = F_{ij} dX_j \quad i, j \in \{1, 2, 3\} \quad (1)$$

It can be shown (Holzapfel, 2001) that the tensor \mathbf{F} can be uniquely decomposed into a *pure rotation* and a *pure stretch*. In addition, the determinant of \mathbf{F} represents the ratio between the volume in the deformed configuration and the volume in the reference configuration. Hence, in the case of incompressible media, $J \equiv \det \mathbf{F} = 1$.

The eigenvalues of \mathbf{F} , namely λ_i , $i \in 1, 2, 3$, are called the *principal stretches*. The corresponding eigenvectors are called *principal direction of stretch* and define an orthonormal basis along which the principal stretches are measured.

The invariants of the tensor \mathbf{B} are called *strain invariants* and are defined as:

$$I_1(\mathbf{B}) = B_{ii} = \lambda_1^2 + \lambda_2^2 + \lambda_3^2 \quad (2)$$

$$I_2(\mathbf{B}) = \frac{1}{2}(B_{ii}B_{jj} - B_{ji}B_{ij}) = \lambda_1^2\lambda_2^2 + \lambda_2^2\lambda_3^2 + \lambda_1^2\lambda_3^2$$

$$I_3(\mathbf{B}) = \det \mathbf{B} = \lambda_1^2\lambda_2^2\lambda_3^2$$

Having defined principal stretches and invariants, the incompressibility constraint yields:

$$J \equiv \det \mathbf{F} = \lambda_1\lambda_2\lambda_3 = 1 \quad (3)$$

$$\Rightarrow \lambda_3 = (\lambda_1\lambda_2)^{-1}$$

$$I_3(\mathbf{B}) = 1 \quad (4)$$

Regarding the formulation of the constitutive equations, the majority of nonlinear elastic models assume a strain energy function written either in terms of strain invariants, such that $W = f(I_1, I_2, I_3)$, or in terms of principal stretches, such that $W = f(\lambda_1, \lambda_2, \lambda_3)$. Naturally, in the case of incompressible materials, one can write the strain energy only as a function of two independent stretches or two independent invariants respectively. For instance $W_R(\lambda_1, \lambda_2) = f(\lambda_1, \lambda_2, \lambda_1^{-1}\lambda_2^{-1})$. Concerning invariant-based strain energy functions, a general representation was proposed by Rivlin (1948):

$$W_R = \sum_{p,q=0}^{\infty} C_{pq} (I_1 - 3)^p (I_2 - 3)^q \quad (5)$$

where C_{pq} are material parameters to be determined experimentally, i.e. curve fitted over experimental stress/stretch data (see Sec. II). By only keeping either the first term or the first two terms in Eq. 5, the following models are obtained

$$W_{NH} = C_{10}(I_1 - 3) \quad \text{Neo-Hookean model} \quad (6)$$

$$W_{MR} = C_{10}(I_1 - 3) + C_{01}(I_2 - 3) \quad \text{Mooney-Rivlin model} \quad (7)$$

which are referred in the literature as *Neo-Hookean* (NH) and *Mooney-Rivlin* (MR) models. The so-called *Yeoh* model (Yeoh, 1990) is also a particular form of the Eq. 5 and depends solely on I_1 . For further details of the Yeoh model and for additional invariant-based strain energy formulations, the interested reader can refer to Holzapfel (2001). Concerning stretch-based strain energy functions, a well known model was proposed by Ogden (1972):

$$W_O(\lambda_1, \lambda_2) = \sum_{p=1}^N \frac{\mu_p}{\alpha_p} (\lambda_1^\alpha + \lambda_2^\alpha + \lambda_1^{-\alpha} \lambda_2^{-\alpha} - 3) \quad \text{Ogden model} \quad (8)$$

where N is the model's order and μ_p, α_p are material parameters to be determined experimentally. Considerations of physically realistic response and material stability lead to the inequalities:

$$\mu_p \alpha_p > 0 \quad p = 1, \dots, N (\text{no sum over } i) \quad (9)$$

$$\sum_{p=1}^N \mu_p \alpha_p = 2\mu \quad (10)$$

where $\mu > 0$ is the shear modulus of the material in its reference configuration. Note that the condition given by Eq. 9 is NOT necessary for every i if $N \geq 3$ (Ogden et al., 2004). Regarding the connection between the different formulations, it is interesting to point out that the NH and MR models of Eq. 6 and Eq. 7 can be deduced from Eq. 8, by setting $N = 1, \alpha_1 = 2$ and $N = 2, \alpha_1 = 1, \alpha_2 = 2$, respectively:

$$\begin{aligned} W_{MR} &= C_{10}(I_1 - 3) + C_{01}(I_2 - 3) \quad (11) \\ &= \frac{\mu_1}{2} (\lambda_1^2 + \lambda_2^2 + \lambda_1^{-2} \lambda_2^{-2} - 3) - \frac{\mu_2}{2} (\lambda_1^{-2} + \lambda_2^{-2} + \lambda_1^2 \lambda_2^2 - 3) \end{aligned}$$

where $C_{10} = \mu_1/2$ and $C_{01} = -\mu_2/2$. Having defined a strain energy function for an *incompressible* medium in terms of invariants or stretches, the Cauchy stress tensor can be found by (Holzapfel, 2001):

$$\sigma_{ij} = -\bar{p} \delta_{ij} + 2B_{ij} \frac{\partial W_R}{\partial I_1} - 2B_{ij}^{-1} \frac{\partial W_R}{\partial I_2} \quad \text{Invariant-based model} \quad (12)$$

$$\sigma_{ij} = -\bar{p} \delta_{ij} + F_{ik} \frac{\partial W_O}{\partial F_{jk}} \quad \text{Stretch-based model} \quad (13)$$

The scalar δ_{ij} is the Kronecker delta whereas the scalar \bar{p} is an indeterminate Lagrange multiplier which arises from the imposition of the incompressibility constraint $J - 1 = 0$. Note that the scalar \bar{p} may only be determined from equilibrium conditions or boundary conditions and represents a reaction stress which is workless for every motion and deformation that are compatible with the incompressibility constraint. In practice, it can be physically interpreted

as a hydrostatic pressure (that in fact does not produce any deformation on perfectly incompressible materials).

The first Piola-Kirchoff (or nominal or engineering) (PK) stress is simply given by:

$$P_{ij} = \sigma_{il} F_{il}^{-1} \quad (14)$$

The PK stress represents a force measure per unit surface area defined in the reference (undeformed) configuration. When testing rubber, this is a typical stress measurement since the force is constantly monitored via the load cell whereas the cross-sectional area is usually measured in the reference configuration only.

2.2 Rubber testing under pure homogeneous deformations

Concerning standardized tests for rubber characterization, particular loading conditions are applied such that the mathematical relation between stress and deformation becomes relatively simple. In this context, one defines as *pure homogeneous deformations* the deformations for which the strain magnitude does not vary with position in the body and the principal axes of stretch do not vary in direction relative to an inertial frame either with position in the body or with strain. In such a case, the deformation gradient tensors during deformation can be chosen as being always diagonal with diagonal elements being the principal stretches:

$$F_{ij} = \lambda_j \delta_{ij} \Rightarrow \begin{cases} x_1 = \lambda_1 X_1 \\ x_2 = \lambda_2 X_2 \\ x_3 = \lambda_3 X_3 \end{cases} \quad (15)$$

Typical pure homogeneous deformations are uniaxial (simple) tension/compression, equibiaxial tension/compression, and planar tension/compression (Ogden, 1972). Planar tension is also named pure shear mode of loading. In these cases, the associated true stress tensors is always diagonal with diagonal elements being the principal true stresses:

$$\sigma_i = -\bar{p} + 2 \frac{\partial W_R}{\partial I_1} \lambda_i^2 - 2 \frac{\partial W_R}{\partial I_2} \lambda_i^{-2} \quad \text{Invariant-based model} \quad (16)$$

$$\sigma_i = -\bar{p} + \lambda_i \frac{\partial W_O}{\partial \lambda_i} \quad \text{Stretch-based model} \quad (17)$$

In the same manner, the nominal stress tensor is diagonal with diagonal elements being the principal PK stresses:

$$P_i = \sigma_i \lambda_i^{-1} \quad i \in \{1, 2, 3\} \quad (18)$$

By simply introducing Eqs. 8 in Eqs. 16, the following expressions are trivially found:

$$\sigma_i = \sum_{p=1}^N \mu_p \lambda_i^{\alpha_p} - \bar{p} \quad (19)$$

Recalling that the NH and MR models can be seen as particular forms of the Ogden model (Eq. 8), the expression of Eq. 19 will be used in the following for the general calculation of the principal stresses.

As previously done by Ogden (1972), the mathematical forms to which Eqs. 19 reduces in uniaxial tension/compression, equibiaxial tension/compression and planar tension/compression (Fig. 2) are derived explicitly. In all these cases, Eq. 19 is directly applied instead of Eq. 13.

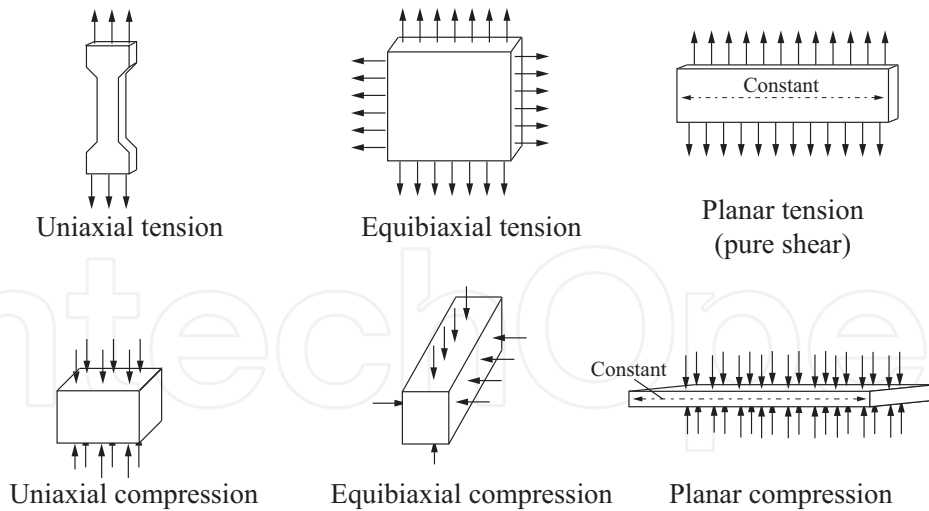


Fig. 2. Schematics of uniaxial tension/compression, equibiaxial tension/compression and pure shear. Adapted from Bhashyam (2002).

2.2.1 Uniaxial tension/compression

Citing from Ogden (1972), let $\lambda_1 = \lambda$ be the stretch ratio in the direction of elongation and $\sigma_1 = \sigma_S$ the corresponding principal Cauchy stress. The other two principal stresses are zero since no lateral forces are applied, i.e. $\sigma_2 = \sigma_3 = 0$. Hence, by virtue of the incompressibility constraint, $\lambda_2 = \lambda_3 = \lambda^{-\frac{1}{2}}$. Using Eq. 19 and eliminating \bar{p} yields:

$$\sigma_S = \sigma_1 = \sum_{p=1}^N \mu_p (\lambda^{\alpha_p} - \lambda^{-\frac{\alpha_p}{2}}) \quad (20)$$

Note that the condition of compression is characterized by $0 < \lambda_1 < 1$ and leads to negative stress values.

2.2.2 Equibiaxial tension/compression

Citing from (Ogden, 1972), in equibiaxial tension/compression two of the principal stresses are equal. For instance $\sigma_2 = \sigma_3 = \sigma_E$ whereas $\sigma_1 = 0$. The corresponding stretches are $\lambda_2 = \lambda_3 = \lambda$ whereas $\lambda_1 = \lambda^{-2}$. Using Eq. 19 and eliminating \bar{p} yields:

$$\sigma_E = \sum_{p=1}^N \mu_p (\lambda^{\alpha_p} - \lambda^{-2\alpha_p}) \quad (21)$$

Note that the condition of compression is characterized by $0 < \lambda_2 = \lambda_3 < 1$ and leads to negative stress values.

2.2.3 Planar tension/compression (pure shear)

Citing from Ogden (1972), in planar tension/compression one of the principal extension ratios is held fixed, say $\lambda_3 = 1$. Setting $\lambda_1 = \lambda$ and $\lambda_2 = \lambda^{-1}$, the stress-strain relations of Eq. 19 reduces to:

$$\sigma_{P1} = \sum_{p=1}^N \mu_p (\lambda^{\alpha_p} - \lambda^{-\alpha_p}) \quad \sigma_{P2} = \sum_{p=1}^N \mu_p (1 - \lambda^{-\alpha_p}) \quad \sigma_{P3} = 0 \quad (22)$$

Once again, the condition of compression is characterized by $0 < \lambda_1 < 1$ and leads to negative stress values.

2.2.4 General expression for the PK stress

Concerning PK stress, simple calculations starting from Eqs. 20, 21, 22 lead to the following expression, which turns useful when numerically fitting experimental stress-stretch curves:

$$P = f_{PK}(\lambda, K, \mathbf{C}) \quad (23)$$

$$= \sum_{p=1}^N (\mu_p (\lambda^{\alpha_p - 1}) - \lambda^{(-1 - \alpha_p / K)})$$

where $K = 2$ for uniaxial tension/compression, $K = 1/2$ for equibiaxial tension/compression, $K = 1$ for pure shear, and $\mathbf{C} = [\mu_1, \alpha_1, \mu_2, \alpha_2 \dots \mu_N, \alpha_N]^t$ is a vector of (unknown) material parameters.

2.3 Equivalence of different modes of deformation

As reported in Ogden et al. (2004), multiple modes of deformation are required to assess the material constants that define the hyperelastic stress-strain relationship in quasi-static conditions. Nonetheless, in the case of incompressible materials, some modes of deformation theoretically provide the same information. In particular, the following modes of deformation are equivalent:

- Uniaxial Tension and Equibiaxial Compression.

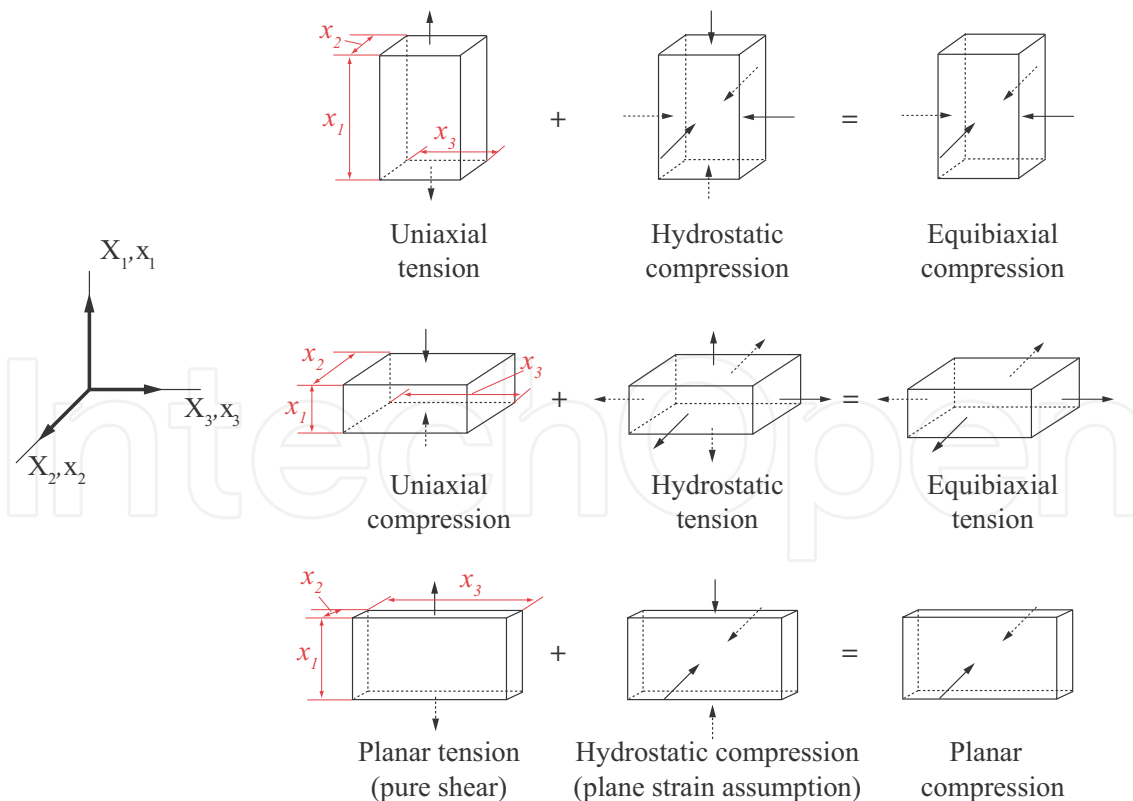


Fig. 3. Equivalence of different modes of deformation. Adapted from Bhashyam (2002).

- Uniaxial Compression and Equibiaxial Tension.
- Planar Tension and Planar Compression.

These equivalences hold as long as any hydrostatic pressure superimposed to any stress field arising in the specimen does not affect the deformation field. The concept is well explained in Fig. 3. It is interesting to point out that the equivalence between equibiaxial tests and compression tests turns useful when an equibiaxial test rig is not available. In fact, simple tension/compression and pure shear tests can be easily performed by means of common tensile stages (see, for instance, Figs. 4(a) and 4(b)). On the other hand, pure compression requires the use of frictionless plates, which are rather difficult to achieve in practice. Hence, some authors (e.g. Day & Miller. (2000)) suggest that equibiaxial tension tests should be better suited to achieve information about the material behavior under compressive loads.

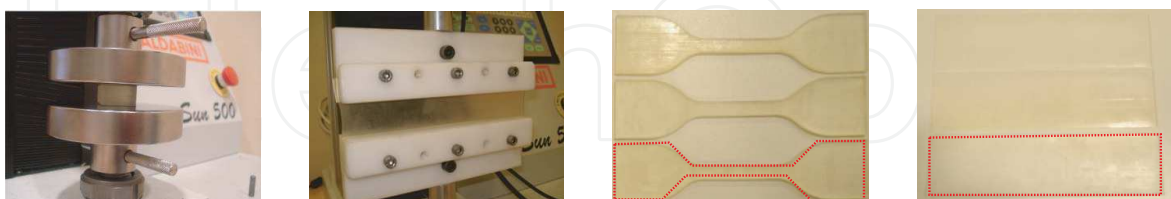
3. Determination of the material hyperelastic parameters

The PP under investigation is named *Tango Plus*® *Fullcure 930* (hardness 27 Shore A). This material is compatible with Polyjet processes and it is currently commercialized by Objet Geometries in two colors (yellow or black) having identical mechanical properties. The tests performed for material characterization are cyclic Uniaxial Tension (UT), Uniaxial Compression (UC) and Pure Shear (PS)¹. As said, the material is considered isotropic and incompressible. Note, once again, that the hypothesis of isotropy is a strong simplification of the physical system yet supported by macroscopic experimental evidence.

The specimens were mounted on a tensile stage (GALDABINI SUN 500, Figs. 4(a) and 4(b)) capable of measuring lengths and tensile/compressive forces with an accuracy of less than 10 μ m and 0.01N respectively; the room temperature was 21°C; the velocity of the tensile stage was set to 10 mm/min.

The specimen geometry and loading cycles were as it follows:

- Uniaxial compression (Fig. 4(a)): parallelepiped test piece of size 18.69 x 21.67 x 21.786 mm subjected to two loading cycles at increasing strain level, i.e. 25%, 50%, (four loading cycles in total). Before the compression test, petroleum jelly was applied on the loading plates of the tensile stage to reduce friction at the contact interface.
- Uniaxial tension (Fig. 4(c)): standardized 2 mm thick dumb-bell test piece with test length of 25 mm subjected to three loading cycles at increasing strain level, i.e. 25%, 80%, 120% (nine loading cycles in total);



(a) Uniaxial compression. Test rig: GALDABINI SUN 500
 (b) Pure shear. Test rig: GALDABINI SUN 500
 (c) Uniaxial tension dumb-bell test pieces
 (d) Pure shear test pieces

Fig. 4. Test specimen and test rig.

¹ The standards ISO 37:1994, ISO 7743:1989 and ISO 2393:1994 were followed during sample preparation and testing.

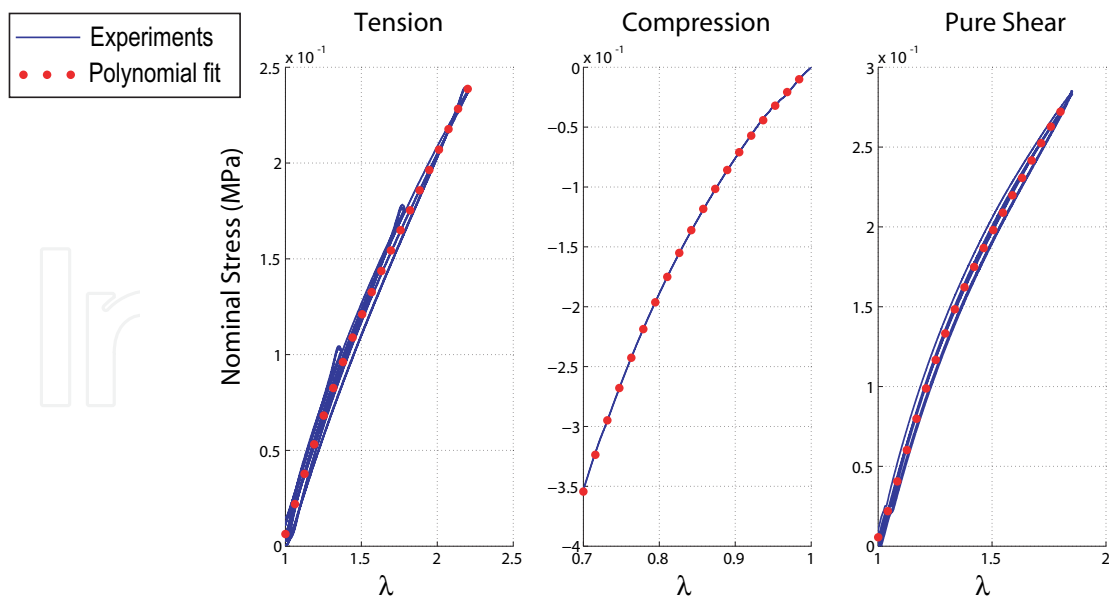


Fig. 5. Nominal stress vs stretch test data for uniaxial compression, uniaxial tension and pure shear.

- Pure shear (Figs. 4(b) and 4(d)): 2 mm thick rectangular test piece of 200 x 20mm subjected to three loading cycles at increasing strain level, i.e. 25%, 80%, (six loading cycles in total); the specimen dimensions are chosen in order to make the deformation along X_3 negligible (refer to Fig. 3).

Test data, reported in Fig. 5, are then numerically fitted with a 5 – th order degree polynomial (dotted curve in Fig. 5) which has been used to identify the strain-energy parameters.

Let $\lambda^{ut} = [\lambda_1^{ut} \dots \lambda_k^{ut} \dots \lambda_r^{ut}]^T \in \mathbb{R}^r$, $\lambda^{uc} = [\lambda_1^{uc} \dots \lambda_k^{uc} \dots \lambda_s^{uc}]^T \in \mathbb{R}^s$, $\lambda^{ps} = [\lambda_1^{ps} \dots \lambda_k^{ps} \dots \lambda_t^{ps}]^T \in \mathbb{R}^t$ be the vectors of experimental stretch values imposed during UT, UC, and PS respectively (i.e. $k = 1 \dots r$, $k = 1 \dots s$, $k = 1 \dots t$ are the numerical indices of the data points concerning UT, UC and PS respectively). Let $\bar{\mathbf{P}}^{ut} \in \mathbb{R}^r$, $\bar{\mathbf{P}}^{uc} \in \mathbb{R}^s$, $\bar{\mathbf{P}}^{ps} \in \mathbb{R}^t$ be the corresponding values of experimental PK stress (referring to the polynomial fit, dotted curve in Fig. 5). Hence $(\lambda^{ut}, \bar{\mathbf{P}}^{ut})$, $(\lambda^{uc}, \bar{\mathbf{P}}^{uc})$, $(\lambda^{ps}, \bar{\mathbf{P}}^{ps})$ represent given pairs of experimental data.

In addition, let $\mathbf{P}^{ut} = [P_1^{ut} \dots P_k^{ut} \dots P_r^{ut}]^T \in \mathbb{R}^r$, $\mathbf{P}^{uc} = [P_1^{uc} \dots P_k^{uc} \dots P_s^{uc}]^T \in \mathbb{R}^s$, $\mathbf{P}^{ps} = [P_1^{ps} \dots P_k^{ps} \dots P_t^{ps}]^T \in \mathbb{R}^t$ be the vectors of theoretical PK stress values corresponding to λ^{ut} , λ^{uc} , λ^{ps} during UT, UC, and PS respectively. In particular, the k -th value of each PK stress can be found via Eq. 23 (i.e. $P_k^{ut} = f_{PK}(\lambda_k^{ut}, 2, \mathbf{C})$, $P_k^{uc} = f_{PK}(\lambda_k^{uc}, 2, \mathbf{C})$, $P_k^{ps} = f_{PK}(\lambda_k^{ps}, 1, \mathbf{C})$). The vector \mathbf{C}^* of optimal material parameters can be found by minimizing

$$\min_{\mathbf{C}} S(\mathbf{C}) \quad \text{where}$$

$$\begin{aligned} S(\mathbf{C}) &= \|\mathbf{P}^{ut} - \bar{\mathbf{P}}^{ut}\|_2^2 + \|\mathbf{P}^{uc} - \bar{\mathbf{P}}^{uc}\|_2^2 + \|\mathbf{P}^{ps} - \bar{\mathbf{P}}^{ps}\|_2^2 \\ &= \sum_{k=1}^r [P_k^{ut} - \bar{P}_k^{ut}]^2 + \sum_{k=1}^s [P_k^{uc} - \bar{P}_k^{uc}]^2 + \sum_{k=1}^t [P_k^{ps} - \bar{P}_k^{ps}]^2 \end{aligned} \quad (24)$$

The symbol $\|\cdot\|_2^2$ identifies the squared 2-norm of a vector. For the purposes of the present paper, the function *Lsqcurvefit* in the Optimization Toolbox of MATLAB has been

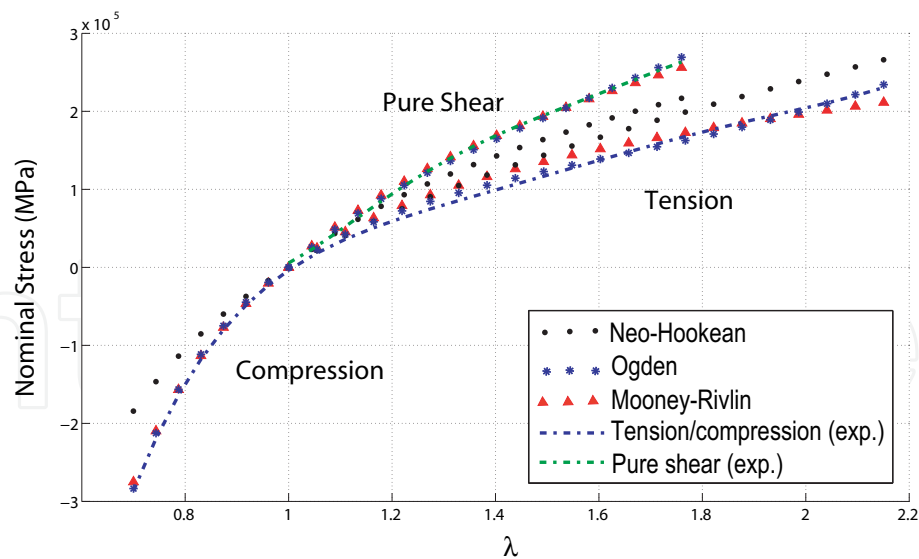


Fig. 6. Nominal stress vs stretch data for uniaxial compression, uniaxial tension and pure shear. Experimental (exp.) data, numerical fitting by means of Neo-Hookean (Eq. 6), Mooney-Rivlin (Eq. 7), and Ogden (Eq. 8) models.

used (Ogden et al., 2004). The MATLAB code concerning the fitting procedure is reported in Appendix I.

Figure 6 shows the best fit of the test data by using the hyperelastic models NH (Eq. 6), MR (Eq. 7), and 4th order Ogden (Eq. 8) models respectively. It can be seen that the NH model is not capable of well capturing the material behavior within the considered stretch range. In order to allow a better comparison of the data fit, a plot of the relative error, e , is reported in Fig. 7 concerning each test. The vector e is calculated as

$$e_k = \frac{|f_{PK}(\lambda_k, K, \mathbf{C}^*) - \bar{P}_k|}{\bar{P}_k} \quad (25)$$

Note that the values of stretch closed to 1 have been discarded in order to avoid very large relative error values due to zero PK stress. In particular, the MR model provides acceptable fitting accuracy (within 10% relative error) whereas a 4th order Ogden model is capable of numerically fitting the data test within 5% relative error. Of course, the relative error can be diminished in case the numerical fitting is restricted to smaller stretch ranges. The constitutive parameters of the PP *Tango Plus*® *Fullcure 930* are shown in Table 1. As a last consideration, it is interesting to note that numerical fits performed over single sets of data (e.g. uniaxial tension) returns unacceptable errors concerning the set of data which have been left out from the fitting procedure (e.g. UT and PS). As an instance, Fig. 8 reports the relative errors concerning UT, UC, and PS for a numerical fit performed over UT only. In such a case, the MR model and the NH model return the same result (i.e. $C_{01} = 0$), with relative errors

Ogden	$\mu_1 = 6.8989e + 5Pa$	$\alpha_1 = 0.0235$
(4 th Order)	$\mu_2 = 2.2271e + 4Pa$	$\alpha_2 = 2.93$
	$\mu_3 = -7.3759e + 4Pa$	$\alpha_3 = -2.7366$
	$\mu_4 = 1.0673e + 3Pa$	$\alpha_4 = 5.5084$
Mooney-Rivlin	$C_{10} = 6.7664e + 4Pa$	$C_{01} = -9.1133e + 4Pa$

Table 1. *Tango Plus*® *Fullcure 930*

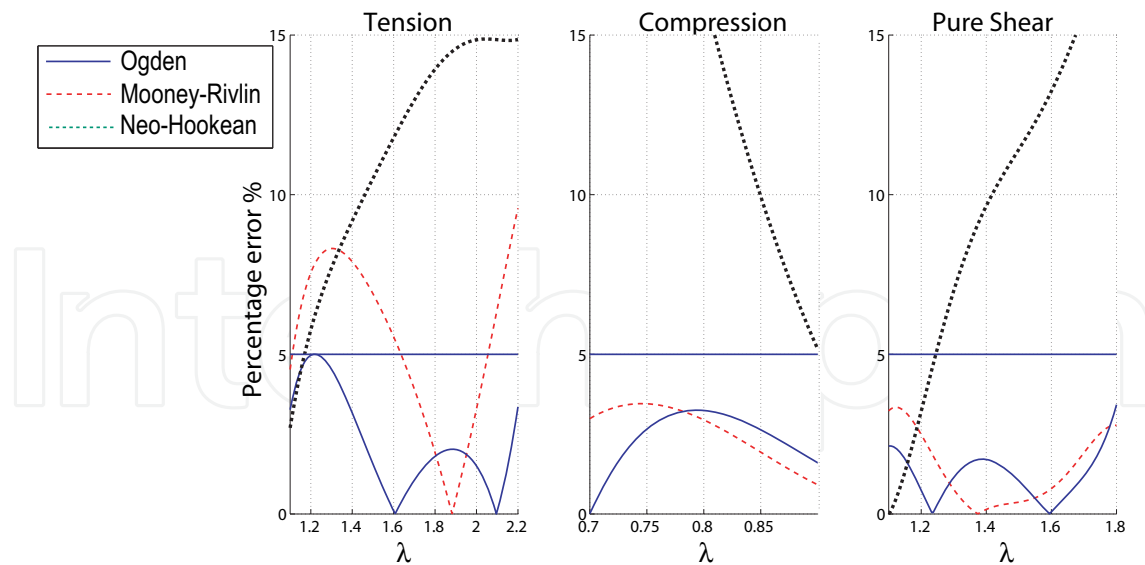


Fig. 7. Percentage error concerning Neo-Hookean (Eq. 6), Mooney-Rivlin (Eq. 7), and Ogden (Eq. 8) models.

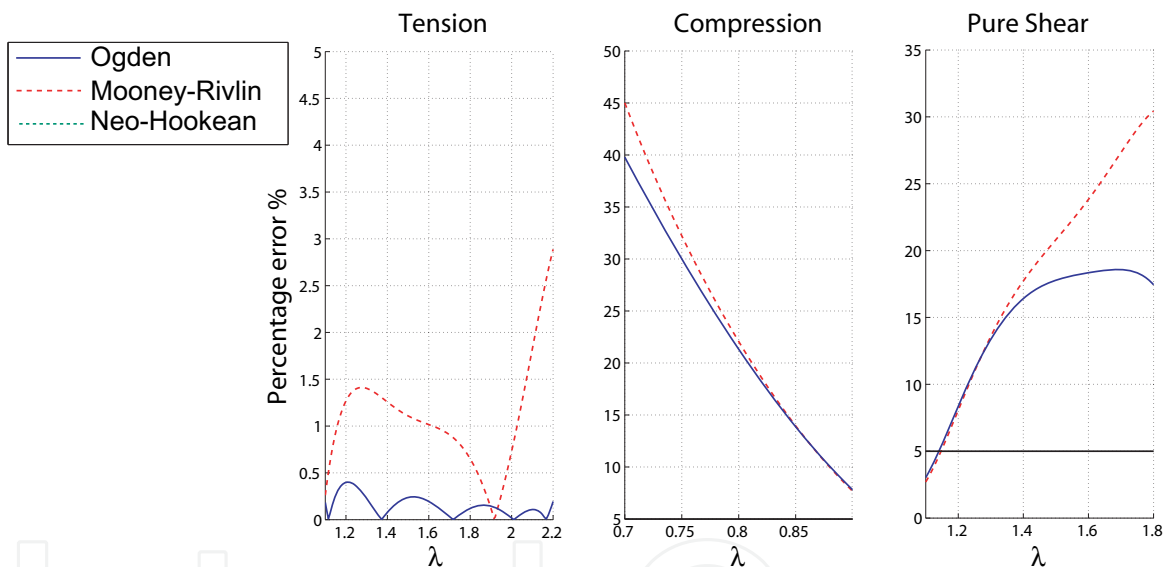


Fig. 8. Percentage error concerning Neo-Hookean (Eq. 6), Mooney-Rivlin (Eq. 7), and Ogden (Eq. 8) models.

concerning UT within 3%. The Ogden model returns relative errors of less than 0.5%. On the other hand, the errors concerning UC and PS become unacceptable.

4. Design case study: soft pads under normal contact load

As a design case study, the nonlinear Finite Elements Analysis (FEA) of soft artificial fingertips (pads) in contact conditions is discussed. The purpose is to test the reliability of the proposed constitutive models when designing soft pads for robotic devices such as anthropomorphic hands, prostheses and orthoses (Berselli & Vassura, 2010; Cabibihan et al., 2009; Dollar & Howe, 2006; Tiezzi & Kao, 2006; Xydas & Kao, 1999). It is self evident that the knowledge of the constitutive behavior of the material composing the pads is fundamental in

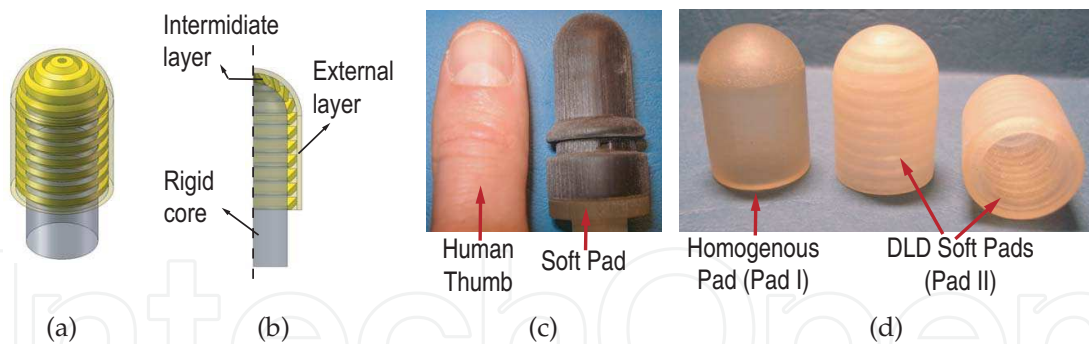


Fig. 9. Soft pad concept and prototype. 3D model (a), longitudinal cross section (b), prototype comparison with human thumb dimensions, material: *Tango Plus Black* (c), comparison between homogenous pad (PAD I) and DLD Pad (Pad II), material: *Tango Plus Yellow* (d).

order to achieve the desired performance and to optimize the overall design.

With respect to previous literature about pad design and modeling, early works concerned hemispherical coreless pads (Li & Kao, 2001; Xydas & Kao, 1999), or homogenous pads shaped over an internal rigid core (Tiezzi & Kao, 2006). Recently (Berselli, Piccinini & Vassura, 2010.), the concept of Differentiated Layer Design (DLD) has been introduced, in order to overcome fundamental limitations of homogenous pads. A DLD pad basically consists in a multi-layered pad constituted by a continuous external skin coupled with a discontinuous internal layer. A 3D model of a DLD pad and its longitudinal cross section are depicted in Figs. 9(a) and 9(b) whereas Figs. 9(c) and 9(d) depict pad prototypes realized by means of AM. In particular, Pad I indicates a homogenous pad whereas Pad II indicates a DLD pad. For given hyperelastic material and pad thickness, a multi-layered solution is used in order to tailor the overall pad compliance to the application by properly shaping the inner discontinuous layer. For instance, particular inner layer morphologies (Berselli et al., 2010) allow to replicate the compliance behavior of the human finger, with great advantage in prosthetic/orthotic applications. In this context, it is fundamental to assess reliable engineering methods and tools to firstly design the optimal morphologies and then to reach the final product. In particular, design optimization through FEA allows the generation of purposely shaped force-displacement curves (Berselli, Piccinini & Vassura, 2010.) whereas, in parallel, the recent availability of elastic materials compatible with AM allows an easy, fast and cheap implementation of items, featuring the very complex shapes that are required to achieve those force-displacement characteristics.

4.1 FEA modelling

The specimens under investigation, similar in size to a human fingertip (Fig. 9(c)), are manufactured using either black or yellow *Tango Plus*® *Fullcure 930* (Fig. 9(c) and 9(d) respectively) and are characterized by a surface hardness similar to that of the human thumb (about 25 Shore A). Concerning the specimen geometries, Pad I (Fig. 9(d) on the left) is composed of a thick layer of homogeneous material shaped around a rigid core whereas Pad II is designed following a DLD concept. The inner layer morphology of Pad II (Fig. 9(d) on the right) is characterized by circumferential ribs connecting the rigid core to the skin layer. Each rib is inclined by 45° with respect to the normal to the external surface, thus transforming normal loads acting on the contact into bending actions applied on each rib. It has been previously shown (Berselli et al., 2010), that a 3mm thick DLD pad represents a substantial

step forward in human finger mimicry in terms of stiffness, when compared to previously published solutions where different materials and higher pad thicknesses were used.

As for the experimental tests, the pads are pushed against a flat surface (rigid wall) while imposed displacement and resultant force are recorded. The rigid wall is made of plexiglass, characterized as a linear elastic material with Young's modulus $E = 3000\text{MPa}$ and Poisson's ratio $\nu = 0.3$. The rigid wall is covered with petroleum jelly before every compression experiment. As for the FEA model, the simulating software is ANSYS Classic 12.0. Geometry and loads allow to adopt a bi-dimensional axis-symmetric model instead of tridimensional ones. PLANE182 is the element used to mesh the model. This bidimensional element has quadrilateral shape, is composed by 4 nodes and ensures good performances when simulating finite deformations. CONTA172 and TARGE169 are the elements chosen for the contact pairs. With regard to solution controls, the element's technology is based on the *Selective Reduced Integration Method* (also named \bar{B} method) that helps to prevent volumetric mesh locking that usually occurs in nearly incompressible models, where a purely hydrostatic pressure can be added without changing the displacement history. In such a case, the displacement field is augmented with a hydrostatic pressure field using a mixed (hybrid) formulation named *Mixed U/P Formulation* (Bhashyam, 2002), that allows to spawn mesh without volumetric

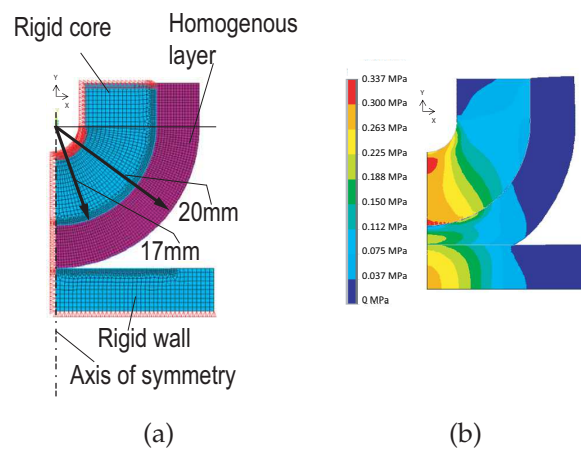


Fig. 10. Homogenous Pad (Pad I). Model mesh (a). Von Mises stress field (MPa) (b)

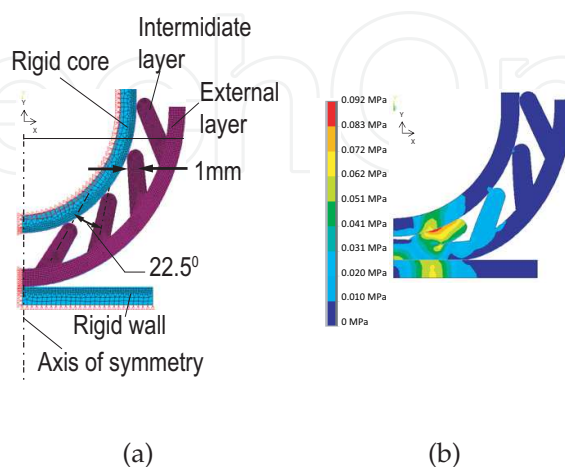


Fig. 11. DLD Pad (Pad II). Model mesh (a). Von Mises stress field (MPa) (b)

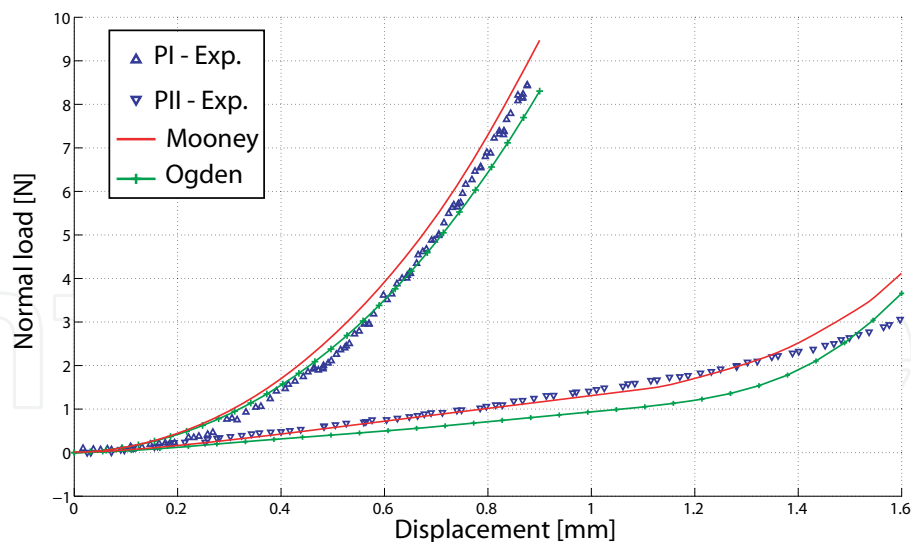


Fig. 12. Displacement (mm) versus Normal Load (N) for uniform Pad I and DLD Pad II. Experimental (exp.) and FEA results achieved with Mooney-Rivlin and Ogden models.

incompressibility problems.

Meshed models and dimensions are shown in Figs. 10(a) and 11(a): green elements for rigid core and rigid wall, purple elements for hyperelastic soft layer, red color for constraints and displacements. In order to investigate the pad response, a displacement in the y (vertical) direction is imposed to the rigid wall and a measurable reaction force is generated on the rigid core on which the soft pad is mounted. The parameters of the Ogden and MR strain energy functions reported in Tab. I have been used within the FEA models of the pads. Similarly to previously published results (Korochkina et al., 2008; Xydas et al., 2000), the simulations include a simple Coulomb friction model which is easier to handle than other friction laws presented in the literature (for example Shallamach (1952)) and allows a better prediction of the experimental values. In order to reproduce the experimental tests, different friction coefficients are used. The friction coefficient between outer pad surface/rigid wall is set to $\mu = 0.1$ whereas the coefficient between inner pad surface/inner rigid core is set to $\mu = 0.4$. Note that petroleum jelly was applied on the rigid wall to reduce friction.

Figures 10(b) and 11(b) shows the Von Mises stress field for Pad I and Pad II, respectively, in the case of Ogden model. At last, Fig. 12 depicts the experimental and numerical compression forces as a function of the indentation displacement. The numerical results achieved by both MR and Ogden model are acceptable.

5. Conclusions

After a discussion about basic concepts of incompressible isotropic hyperelasticity, this chapter reports numerical methods to be used in the design of AM Rubber-Like components and customized products. Within this scenario, the explicit fitting of numerical hyperelastic models to experimental data is a fundamental design issue and a focused engineering method has been exposed.

In particular, it has been shown that numerically fitting a single mode of deformation, (for instance, uniaxial tension) leads to unacceptable results when general modes of deformation must be predicted. Hence, in accordance to the results presented in Ogden et al. (2004), multiple modes of deformation (namely uniaxial tension, uniaxial compression and pure

shear) have been employed for a simultaneous fit. The engineering method have been applied for characterizing *Tango Plus*® *Fullcure 930*, a rubber-like photopolymer widely used in Additive Manufacturing processes. The obtained material data, which fits the specimen deformation up to an imposed strain of 120%, are presented for the first time and can be used when performing finite element analysis. As a design case study, the finite element analysis of soft fingertips for robotic hands have been presented and validated through experiments.

6. Appendix I

The Matlab files `tension.mat`, `compression.mat`, `pure_shear.mat` contains experimental data concerning UT, UC and PS. The first and second columns contain, respectively, the vectors of displacements imposed to the specimens and the corresponding forces as read by the load cell. The following variables are defined:

- `d_UT`, `d_UC`, `d_PS`: displacements imposed during UT, UC, PS respectively.
- `f_UT`, `f_UC`, `f_PS`: force read during UT, UC, PS respectively.
- `L_UT`, `L_UC`, `L_PS`: stretch values during UT, UC, PS respectively.
- `L_max_UT`, `L_max_UC`, `L_max_PS`: maximum imposed stretch value for UT, UC, PS respectively.
- `S`: PK stress calculated via Eq. 23.
- `C=[mu1 alpha1 ... mu4 alpha4]`: Optimal material parameters.
- `P_UT`, `P_UC`, `P_PS`: PK stress values during UT, UC, PS respectively.
- `Pol_UT`, `Pol_UC`, `Pol_PS`: coefficients of the 5 – th order polynomial functions approximating the experimental data (dotted curve in Fig. 5).
- `PKF_UT`, `PKF_UC`, `PKF_PS`: PK stress values corresponding to `L_UT`, `L_UC`, `L_PS` and calculated by means of the 5 – th order polynomial functions whose coefficients are given by `Pol_UT`, `Pol_UC`, `Pol_PS`.
- `X1`, `X2`, `X3`: specimen undeformed dimensions.
- `r`, `s`, `t`: number of experimental points (i.e. r, s, t in Eq. 24). If any of these values is set to 0, the corresponding test is discarded.

The following Matlab script is used to identify a polynomial fit of UT experimental data. Similar scripts are used for UC and PS experimental data.

```

1  %read uniaxial test data
2  load('tension.mat')
3  d_UT=tension(:,1); %imposed displacement
4  f_UT=tension(:,2); %force in Newton
5
6  %undeformed dimensions in meters
7  X1=25e-3; X2=6e-3; X3=3e-3;
8
9  %calculation of stretch vector and corresponding nominal stress
10 L_UT=(d_UT+X1)/X1; %Stretch values
11 P_UT=f_UT./(X2*X3); %Engineering stress
12
13 %polynomial fit of experimental stress-stretch curve
14 Pol_UT=polyfit(L_UT,P_UT,5); %fifth order polynomial

```

The following script recall the non-linear least square algorithm `Lsqcurvefit` in the Optimization Toolbox of MATLAB.

```

1  r=220; s=70; t=180;
2
3  L_max_UT=2.2; L_max_UC=0.7; L_max_PS=1.8;
4
5  %calculate tension data to be fitted with Ogden function
6  L_UT=linspace (1, L_max_UT, r); %stretch values equally spaced ...
   between 1 and 'L_max_UT'
7  if r==0
8      L_UT=[];
9  end
10 PKF_UT=polyval(Pol_UT,L_UT); %PK stress corresponding to 'L_UC'.
11
12 %calculate compression data to be fitted with Ogden function
13 L_UC=linspace (L_max_UC, 1, s); %stretch values equally spaced ...
   between 'L_max_UT' and 1
14 if s==0
15     L_UC=[];
16 end
17 PKF_UC=polyval(Pol_UC,L_UC); %PK stress corresponding to 'L_UC'.
18
19 %calculate pure shear data to be fitted with Ogden function
20 L_PS=linspace (1, L_max_PS, t); %stretch values equally spaced ...
   between 1 and 'L_max_PS'
21 if t==0
22     L_PS=[];
23 end
24 PKF_PS=polyval(Pol_PS,L_PS); %PK stress corresponding to 'L_PS'.
25
26 %Calculation of optimal material parameters
27 STRETCH=[L_UT L_UC L_PS]; %Overall stretch vector
28 STRESS=[PKF_UT PKF_UC PKF_PS]; %Overall stress vector
29 C0 = [2.1007e+005, 8, 6.3623e-008, 26, -5.7116e+004, -25.6149 1 1]; ...
   %Initial guess
30 lb = [0, 0, 0, 0, -inf, -inf,0,0]; %Lower bound of the optimal ...
   solution vector
31 ub = [inf, inf, inf, inf, 0, 0,inf,inf]; %Upper bound of the optimal ...
   solution vector
32 optnew = optimset('DiffMaxChange',0.000001,'DiffMinChange',1e-15,...
33     'TolFun',1e-15, 'TolX',1e-15,'MaxFunEvals',3000,'MaxIter',3000); ...
   %Curve fit options
34 [C] = lsqcurvefit(@energy,C0,STRETCH,STRESS,lb,ub,optnew) %optimal ...
   solution

```

The following function is connected to the previous script and returns PK stress calculated via Eq. 23.

```

1 function S = energy(C,L)
2 global r s t
3
4 L_tot=L %input stretch vector
5
6 %material constants
7 mu1=C(1); alpha1=C(2);
8 mu2=C(3); alpha2=C(4);
9 mu3=C(5); alpha3=C(6);
10 mu4=C(7); alpha4=C(8);
11
12 %K=1 for pure shear, K=2 for simple tension/compression
13 if t==0
14     K=[2*ones(r+s,1)']
15 elseif (r+s)==0
16     K=[1*ones(t,1)']
17 else
18     K=[2*ones(r+s,1)' 1*ones(Npunti_sh,1)']
19 end
20
21 S=...
22 mu1.*(L.^(alpha1-1)-L.^(-(1+alpha1./K)))+ ... %Strain energy first term
23 mu2.*(L.^(alpha2-1)-L.^(-(1+alpha2./K)))+ ... %Strain energy second term
24 mu3.*(L.^(alpha3-1)-L.^(-(1+alpha3./K)))+ ... %Strain energy third term
25 mu4.*(L.^(alpha4-1)-L.^(-(1+alpha4./K))); %Strain energy fourth term

```

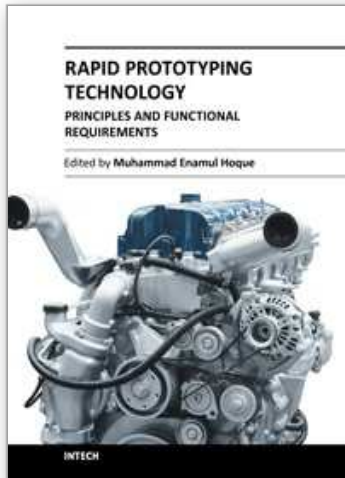
7. Acknowledgment

The authors wish to acknowledge the contribution of Dr. M. Piccinini.

8. References

- Berselli, G., Piccinini, M. & Vassura, G. (2010.). On designing structured soft covers for robotic limbs with predetermined compliance, *Proc. ASME IDETC 2010, International Design Engineering Technical Conferences*, ISBN 978-0-7918-3881-5, Montreal, Canada.
- Berselli, G. & Vassura, G. (2009.). Differentiated layer design to modify the compliance of soft pads for robotic limbs, *Proc. IEEE ICRA2009, International Conference on Robotics and Automation*. pp. 1247–1252, ISSN: 1050-4729, Kobe, Japan.
- Berselli, G. & Vassura, G. (2010). From dexterous robotic hands to prosthetic hands issues for design and thechology transfer, *Grasping the Future: Advances in Powered Upper Limb Prosthetics, Bemtham (in press)* .
- Berselli, G. et al. (2010). Engineering design of fluid-filled soft covers for robotic contact interfaces: Guidelines, nonlinear modeling and experimental validation, *IEEE Transactions on Robotics (in press)* .
- Bhashyam, G. R. (2002). *ANSYS Mechanical, A Powerful Nonlinear Simulation Tool*, Ansys, Inc.
- Cabibihan, J., S. Pattofatto, M. J., Benallal, A. & Carrozza, M. (2009). Towards humanlike social touch for sociable robotics and prosthetics: Comparisons on the compliance, conformance and hysteresis of synthetic and human fingertip skins, *International Journal of Social Robotics* 1(1): 29–40, DOI: 10.1007/s12369-008-0008-9.

- Day, J. R. & Miller, K. (2000). Equibiaxial stretching of elastomeric sheets: an analytical verification of experimental technique., *Proceedings of ABAQUS 2000 User's Conference*, Newport, Rhode Island, May 30-June 2, 2000.
- Dollar, A. & Howe, R. (2006). A robust compliant grasper via shape deposition manufacturing, *IEEE/ASME Transactions on Mechatronics* 11(2): 154–161, ISSN: 1083-4435.
- Gibson, I., Rosen, D. & Stucker, B. (2010). *Additive Manufacturing Technologies: Rapid Prototyping to Direct Digital Manufacturing*, Springer Science and Business Media, ISBN: 978-1-4419-1119-3, Boston, MA.
- Holzappel, G. A. (2001). *Nonlinear Solid Mechanics: A Continuum Approach for Engineering*, John Wiley and Sons, ISBN 0471-82304, New York.
- Korochkina, T., Jewell, E., Claypole, T. & Gethin, D. (2008). Experimental and numerical investigation into nonlinear deformation of silicone rubber pads during ink transfer process, *Polymer Testing* 27(6): 778–791, ISSN: 0142-9418.
- Li, Y. & Kao, I. (2001). A review of modeling of soft-contact fingers and stiffness control for dextrous manipulation in robotics, *Proceedings of IEEE ICRA, International Conference on Robotics and Automation* 3: 3055–3060 vol.3, ISBN: 0-7803-6576-3.
- Ogden, R. W. (1972). Large deformation isotropic elasticity: on the correlation of theory and experiment for incompressible rubber-like solids, *Proceedings of the Royal Society of London* A-326: 565–584, DOI: 10.1098/rspa.1972.0026.
- Ogden, R. W., Saccomandi, G. & Sgura, I. (2004). Fitting hyperelastic models to experimental data, *Computational Mechanics* 34(6): 484–502, DOI: 10.1007/s00466-004-0593-y.
- Piccinini, M., Berselli, G., Zucchelli, A. & Vassura, G. (2009.). Predicting the compliance of soft fingertips with differentiated layer design: A numerical and experimental investigation, *Proc. IEEE ICAR, International Conference on Advanced Robotics*, pp. 1–6, Munich, Germany.
- Rivlin, R. (1948). Large elastic deformations of isotropic materials: Further developments of general theory., *Philosophical Transactions of the Royal Society of London, Series A* 241: 379–397, doi: 10.1098/rsta.1948.0024.
- Shallamach, A. (1952). The load dependence of rubber friction., *Proc. of the Physical Society* 65(393B): 658–661, doi: 10.1088/0370-1301/65/9/301.
- Tiezzi, P. & Kao, I. (2006). Characteristics of contact and limit surface for viscoelastic fingers, *Proceedings of IEEE ICRA, International Conference on Robotics and Automation*, pp. 1365–1370, ISSN: 1050-4729, Orlando, Florida.
- Xydas, N., Bhagavat, M. & Kao, I. (2000). Study of soft-finger contact mechanics using finite elements analysis and experiments, *Proc. IEEE ICRA, International Conference on Robotics and Automation*. 3: 2179–2184, ISBN: 0-7803-5886-4, San Francisco, CA , USA.
- Xydas, N. & Kao, I. (1999). Modeling of contact mechanics and friction limit surface for soft fingers in robotics, with experimental results, *International Journal of Robotic Research* 18(8): 941–950, doi: 10.1177/02783649922066673.
- Yeoh, O. H. (1990). Characterization of elastic properties of carbon-black-filled rubber vulcanizates, *Rubber Chemistry and Technology* 63: 792–805, ISSN 0035-9475.



Rapid Prototyping Technology - Principles and Functional Requirements

Edited by Dr. M. Hoque

ISBN 978-953-307-970-7

Hard cover, 392 pages

Publisher InTech

Published online 26, September, 2011

Published in print edition September, 2011

Modern engineering often deals with customized design that requires easy, low-cost and rapid fabrication. Rapid prototyping (RP) is a popular technology that enables quick and easy fabrication of customized forms/objects directly from computer aided design (CAD) model. The needs for quick product development, decreased time to market, and highly customized and low quantity parts are driving the demand for RP technology. Today, RP technology also known as solid freeform fabrication (SFF) or desktop manufacturing (DM) or layer manufacturing (LM) is regarded as an efficient tool to bring the product concept into the product realization rapidly. Though all the RP technologies are additive they are still different from each other in the way of building layers and/or nature of building materials. This book delivers up-to-date information about RP technology focusing on the overview of the principles, functional requirements, design constraints etc. of specific technology.

How to reference

In order to correctly reference this scholarly work, feel free to copy and paste the following:

Giovanni Berselli, Rocco Vertechy, Marcello Pellicciari and Gabriele Vassura (2011). Hyperelastic Modeling of Rubber-Like Photopolymers for Additive Manufacturing Processes, Rapid Prototyping Technology - Principles and Functional Requirements, Dr. M. Hoque (Ed.), ISBN: 978-953-307-970-7, InTech, Available from: <http://www.intechopen.com/books/rapid-prototyping-technology-principles-and-functional-requirements/hyperelastic-modeling-of-rubber-like-photopolymers-for-additive-manufacturing-processes>

INTECH
open science | open minds

InTech Europe

University Campus STeP Ri
Slavka Krautzeka 83/A
51000 Rijeka, Croatia
Phone: +385 (51) 770 447
Fax: +385 (51) 686 166
www.intechopen.com

InTech China

Unit 405, Office Block, Hotel Equatorial Shanghai
No.65, Yan An Road (West), Shanghai, 200040, China
中国上海市延安西路65号上海国际贵都大饭店办公楼405单元
Phone: +86-21-62489820
Fax: +86-21-62489821

© 2011 The Author(s). Licensee IntechOpen. This chapter is distributed under the terms of the [Creative Commons Attribution-NonCommercial-ShareAlike-3.0 License](#), which permits use, distribution and reproduction for non-commercial purposes, provided the original is properly cited and derivative works building on this content are distributed under the same license.

IntechOpen

IntechOpen